Schultz P. H. and Merrill R. B., eds.
Multi-ring Basins, Proc. Lunar Planet. Sci. (1981), 12A, p. 181–195.
Printed in U.S.A.

Multi-ring basin formation: Possible clues from impact cratering calculations

P. H. Schultz[1], D. Orphal[2], B. Miller[1], W. F. Borden[2] and S. A. Larson[2]

[1]Lunar and Planetary Institute, 3303 NASA Road 1, Houston, Texas 77058
[2]California Research and Technology, Incorporated, 4049 First Street, Suite 135, Livermore. California 94550

Abstract—Finite-difference codes of impact crater formation (1–2 km diameter) reveal trends that may provide clues for the formation of multi-ringed basins. Early stages of cratering are characterized by non-proportional growth of the crater cavity expressed as a change in the aspect ratio (diameter : depth) from near unity to the final values close to 3 : 1. The aspect ratio appears to depend on impact velocity, and extrapolation of scaling relations to basin-size events suggests that gravity-limited excavation cavities may have been more cylinder-shaped than bowl-shaped. Such a shape is most probable for low-velocity, basin-forming objects. Calculations also indicate that ejecta volume increases in proportion with the cube of cavity dimension. This disparity between non-proportional cavity growth and proportional ejection is attributed to early-stage compression effects. Ejecta at any given range from the impact (<40 crater radii) exhibit a range of two orders-of-magnitude in peak pressures experienced prior to ejection. Although peak pressures appear to depend on impact velocity, ejection velocities (thus the distribution of shocked materials) reflect the cratering flow field, which is generally independent of impact velocity. The distribution of ejecta areal density (mass/area), which represents an effective arrival thickness, exhibits a steep power-law decay with an exponent near −3 near the crater rim decreasing to −2 at ranges beyond 4 crater radii under lunar gravity. The combination of gravity-limited growth for basin-size events and early-time compression effects reduces the total ejecta areal density expected at the final observed basin rim, but the reduced power-law decay indicates that far-rim quantities of ejecta may be significantly greater (relative to the near-rim deposits) than previously proposed. Although extrapolation of such calculations to basin-size events is potentially invalid, such an approach permits defining new questions for future studies.

INTRODUCTION

Finite difference continuum mechanics code calculations permit varying the controlling variables in an impact event and determining basic trends at scales unavailable to experimental analysis. A previous contribution (Orphal *et al.*, 1980) summarized the results of a pair of such calculations for identical projectile/target characteristics but different impact velocities. One calculation considered a relatively low velocity iron impactor (5 km/s); the other, a high velocity iron impactor (15.8 km/s). These two velocities represent an order-of-magnitude difference in the impact energy. The primary purpose was to investigate the generation and transport of impact melt for the two impact energies.

The impact energies involved in this calculation ($\sim 10^{23}$ ergs) are well below the energies believed to be responsible for basin-size events ($\sim 10^{34}$ ergs). Nevertheless, there are several trends that may be fundamental to our understanding of transient cavity formation, ejecta distribution, and ejecta provenance. Just as laboratory experiments and terrestrial impact craters can be extrapolated only with caution, these calculations—as applied to basin-forming events—are used only to raise new questions on a physical basis.

CRATER GROWTH

The calculations are described in more detail in Orphal *et al.* (1980), with the parameters shown in Table 1. They are based on a Lagrangian finite-difference code and carried to relatively late times in the cratering process. The lower velocity impact (5 km/sec and termed NASA-1) produced a crater having a diameter of about 0.9 km and taking approximately 4.2 seconds to form. The higher velocity impact (15.8 km/sec and termed NASA-2) produced a 1.8 km-diameter crater in approximately 5.6 seconds. These quantities are extrapolated after the cratering flow field was well established. The diameter and ejected volume of NASA-2 are slightly smaller (10% and 20%, respectively) than previously reported owing to further study of the output data.

Figure 1 permits comparison of cavity growth and excavation for the two calculations. For both NASA-1 and NASA-2, cavity growth (upper curve) cannot be described by a simple power-law relation. During the earliest stages of formation, cavity volume grows as slightly less than the cube of the transient cavity radius (x). Over most of crater growth, however, relative cavity volume expands as the square (or less) of cavity dimension. Inflection in cavity growth relations occurs between x/R = 0.3 and 0.5 for both NASA-1 and NASA-2 where R is the final crater radius referenced to the pre-impact surface.

The cumulative volume (mass) of material ejected (lower curve) at a given stage in cavity growth exhibits a behavior different from cavity volume. During the early stages of

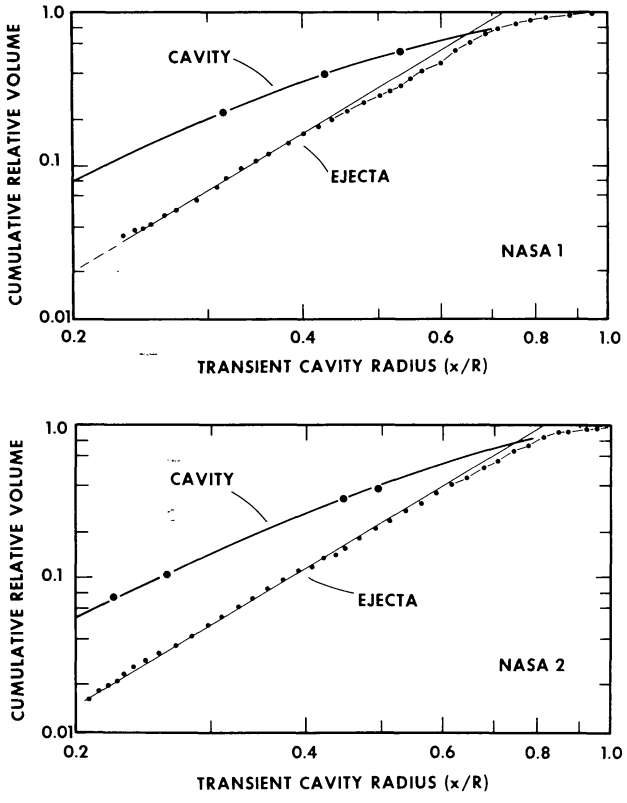

Fig. 1. Comparison of the cavity volume (V_c) and cumulative ejecta volume (V_e) relative to final crater volume (V_C) and total ejecta volume (V_E) as a function of relative crater growth defined by the current radius of the cavity (x) relative to the final radius R. Ejecta are defined as materials passing through the ground surface at a given time. Figure 1a shows the results for NASA-1; Fig. 1b shows the results for NASA-2.

Table 1.

		NASA-1	NASA-2
IMPACT CONDITIONS	Projectile radius	3.12 m	3.12 m
	Projectile mass	1×10^{12} grams	1×10^{12} grams
	Impact velocity	5 km/sec	15.8 km/sec
	Impact momentum	5×10^{17} dyne-sec	15.8×10^{17} dyne-sec
	Impact kinetic energy	1.25×10^{23} ergs (~3 Mt)	1.25×10^{24} ergs (~30 Mt)
	Target	gabbroic anorthosite	half-space
RESULTS *	Radius (*reference to pre-impact surface*)	450 m	900 m
	Depth	315 m	510 m
	Ejecta volume	3.5×10^{7} m^3	2.9×10^{8} m^3
	Crater volume	6.5×10^{7} m^3	5.5×10^{8} m^3

*Estimated on the basis of ballistic extrapolation of flow fields and asymptotic limits of output data.

both calculations, the cumulative ejected fraction is proportional to the cube of crater dimension. However, NASA-1 begins to depart from cubic growth when the cavity has reached approximately 45% of its final size. NASA-2 exhibits a similar but smaller departure at later stages when the crater has reached about 60% of its final size. Near the final stages of formation, both calculations indicate a third change in the mass fraction ejected. NASA-1 exhibits a marked departure from a cubic to a nearly linear relation after the crater is about 70% complete; similarly, NASA-2 changes after about 80% completion.

A cubic relation between cavity volume and cavity radius can be viewed as proportional cavity growth; i.e., the transient cavity expands in shell-like manner without major changes in form. Figure 1 indicates that non-proportional growth occupies most of crater formation. The cumulative ejected fraction, however, essentially grows proportionally, thereby disassociating a simple relation between crater cavity and crater ejecta. Because the displaced volume represented by the crater cavity exceeds the volume of material ejected, the disparity in growth relates to early-time compression. At late stages ($x/R \geq 0.7$), relative cavity growth and relative ejection converge. Figure 2 shows the ratio of

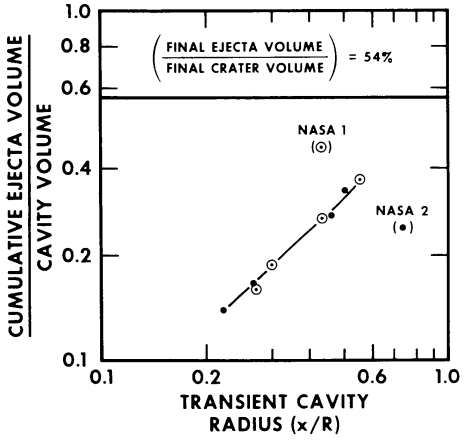

Fig. 2. Comparison of the ratio of material ejected to the amount of material displaced at a given stage (x/R) in crater growth for NASA-1 and NASA-2. Both calculations indicate that only about 50% of the total displaced volume is represented in the total ejecta.

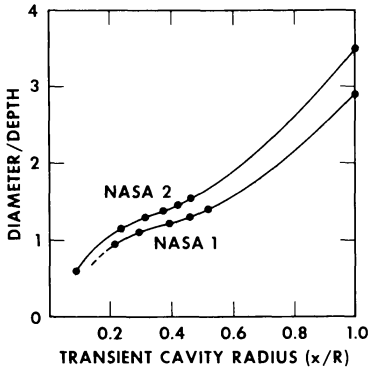

Fig. 3. Comparison of the aspect ratio (diameter : depth) for NASA-1 and NASA-2 at different stages in formation. Continued expansion of the crater radius after maximum crater depth is reached at x/R = 0.45 for both calculations results in a nearly linear increase in the aspect ratio during late stages.

material ejected to cavity volume at a given stage in crater growth. Both calculations reveal that the total volume of ejecta represents only about 50% of the total crater volume. If excavation were to dominate the cratering process at early stages, then the ratio in Fig. 2 would be greater than the final value. This is clearly not the case. Instead, excavation appears to become gradually more important only at late stages.

Cavity growth also can be described by change in crater profile. Figure 3 shows the aspect ratios for NASA-1 and NASA-2 as a function of relative cavity radius. Both calculations exhibit similar trends that can be broken into three stages. At early stages when $x/R < 0.2$, cavity shape is controlled by the penetration of the projectile, and the transient cavity exhibits aspect ratios typically less than unity. Similar features have been reported for similar impact parameters (Ahrens and O'Keefe, 1978). At intermediate stages ($0.2 < x/R < 0.5$), the aspect ratio increases as the cavity expands and the depth approaches its maximum value ($x/R = 0.45$ for both calculations). At late stages ($x/R > 0.5$), crater growth occurs principally by lateral expansion of the crater cavity without a significant increase in crater depth. Figure 3 reveals that the aspect ratio of NASA-2 is consistently larger than NASA-1 by 11% at $x/R = 0.3$, to 19% at $x/R = 0.5$, and finally to 21% at $x/R = 1.0$. It should be noted that late-stage phenomena as described in these calculations are not treated by O'Keefe and Ahrens (1977).

Table 2 summarizes the various aspects of cavity growth for the two calculations. Relative cavity volume and relative cumulative ejecta volume can be described by the following relations:

$$\frac{V_c(x)}{V_C} \propto \left(\frac{x}{R}\right)^{\alpha(x)} \tag{1}$$

$$\frac{V_e(x)}{V_E} \propto \left(\frac{x}{R}\right)^{\beta(x)} \tag{2}$$

Table 2. Summary of crater growth.

Relation	x/R / variable	<0.2	0.2–0.4	0.4–0.6	0.6–0.8	0.8–1.0
$\frac{V_c(x)}{V_C} \propto \left(\frac{x}{R}\right)^{\alpha}$	α_1	>2.5	1.9	1.4	1.2	<1
	α_2	>2.3	2.3	1.9	1.6	~1
$\frac{V_e(x)}{V_E} \propto \left(\frac{x}{R}\right)^{\beta}$	β_1	3	3	2.5	2	<1
	β_2	3	3	3	2.9	<1
D/d	1	<1.0	1.0–1.2	1.2–1.6	1.6–2.2	2.2–2.4
	2	<1.0	1.1–1.4	1.4–2.0	2.0–2.7	2.7–3.5

Subscripts refer to NASA-1 and NASA-2 calculations.

where $V_c(x)$ is the transient cavity volume when the cavity has a radius of x, V_C is the final cavity volume when x = R, $V_e(x)$ is the cumulative ejected material at a cavity radius of x, and V_E is the total amount of material excavated from the crater cavity beyond R. The exponents α and β depend on the stage of growth with representative values shown in Table 2. Table 2 also includes the change in the diameter (D) to depth (d) ratio.

CRATER EJECTA

Although considerable rezoning during the calculations masks the exact nature of the ejected materials, certain information about peak pressures has been retained for each ejected zone. Orphal *et al.* (1980) compare the amount and fate of melted and incompletely melted material generated by the two simulated impact events. The lower velocity NASA-1 calculation indicates that only 0.07 projectile masses of target and projectile material are completely or incompletely melted, all of which is ejected from the cavity during early stages of crater formation. The higher velocity NASA-2 calculation indicates that 3.6 projectile masses are partially vaporized, 7.6 masses become fully melted, and 2.8 masses incompletely melted. In contrast with NASA-1, about half of the melted material remains in the impact cavity.

Further analysis of the data permits specifying the distribution and shocked state of the ejecta. During rezoning, the peak shock pressures in each zone are averaged, but the maximum value prior to rezoning is specifically recorded. Thus, when material is ejected, the data can specify the amount of shock melting or shock vaporization, but can only describe in a general way the peak shock pressures within each averaged zone. Nevertheless, these values are highly useable in indicating zones of extremely high or extremely low averaged peak shock pressures. The number of zones with similar averaged peak pressures arriving at a given range permits describing a "typical" value.

The distribution of averaged peak shock pressures with relative range from each crater is shown in Fig. 4. NASA-1 ejecta (Fig. 4a) exhibit pressures well below values necessary for melting throughout the ejecta to 40R (i.e., 40 crater radii). The small amount of melt generated in this calculation represents a high-velocity component landing 60R from the event. Typical peak pressures tend to skew to the minimum values. Thus, this calculation suggests that most ejecta within 10R have been subjected to peak pressures less than 10 kb. Figure 4b reveals a significantly different distribution for NASA-2. Impact melt occurs essentially throughout the ejecta with the greatest degree of melting found within 3R and beyond 20R. As noted in Orphal *et al.* (1980), about 50% of the total melt is retained within the crater cavity. About 2/3 of the melted material ejected from the crater lands within 3R, only 0.1% of the total ejecta mass. Although the total ejected mass decreases with range, the melt fraction increases, and at 20R, 10% of the ejecta has been shock melted. In contrast with NASA-1, typical peak pressures appear to be offset toward maximum values, and most ejecta within 10R from the rim have been subjected to peak pressures above several kilobars but below 100 kilobars.

Figure 5 allows direct comparison of the peak shock levels at different absolute ballistic ranges for the 5 km/s and 15.8 km/s impacts. If the peak stress solely controls ejection velocity, then impact melt should achieve the same absolute ballistic range in NASA-1 and NASA-2. Figure 5 reveals, however, that peak stress and ballistic range (ejection velocity) are different for the two impact conditions. Although projectile impact velocity controls peak pressures and, therefore, impact-melt generation, ejection velocities and distribution of ejecta appear to be related to the cratering flow field, which is controlled by total impact energy. A clear separation between effects of impact energy and impact momentum requires additional parameterized calculations.

The distribution of ejecta for the NASA-2 calculation is shown in Fig. 6. Ejecta "thickness" is represented here by ballistically transported *mass per unit area* (i.e., areal density). Different bulking effects are partly avoided by normalizing thickness to the thickness at a given range, and effects of rim uplift are largely avoided by referencing thickness to 1.5R rather than the rim. Lateral ejecta transport or secondary cratering

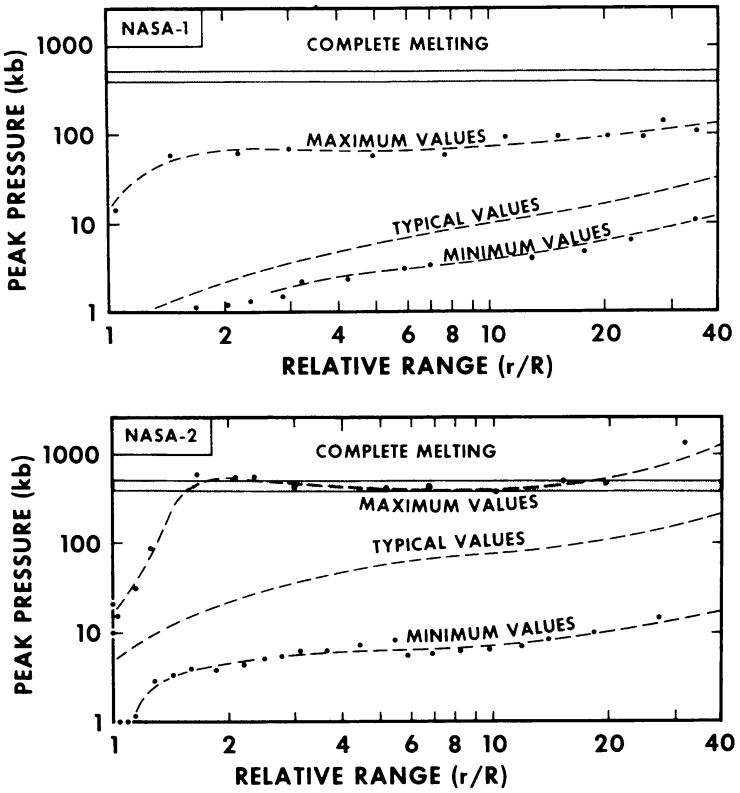

Fig. 4. The distribution of peak shock pressures in the ejecta at different relative ranges from the impact point for NASA-1 (Fig. 4a) and NASA-2 (Fig. 4b). Maximum values reflect an accurate inventory of maximum peak pressures in the ejecta. Typical values reflect the greatest mass of ejecta having the given averaged peak pressure, and minimum values indicate the least averaged peak pressure in the ejecta at a given range. Typical and minimum values reflect the distribution of zone-averaged peak pressures; therefore, they should be used only as a general indication of the peak-pressure history.

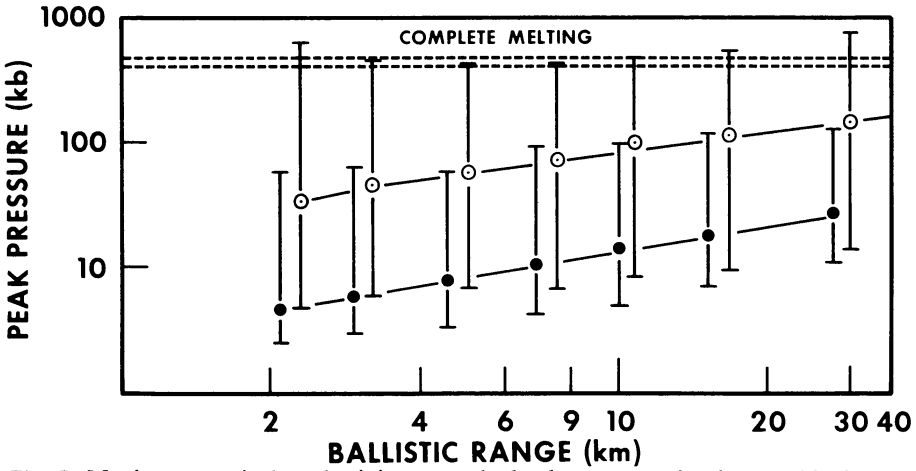

Fig. 5. Maximum, typical, and minimum peak-shock pressures in ejecta achieving the same ballistic range in both NASA-1 and NASA-2 calculations. Maximum and typical values appear to increase nearly an order of magnitude with an order-of-magnitude increase in impact energy, whereas minimum values are nearly unchanged. The small amount of melt produced in the NASA-1 calculation was ejected beyond 60 crater radii from the crater.

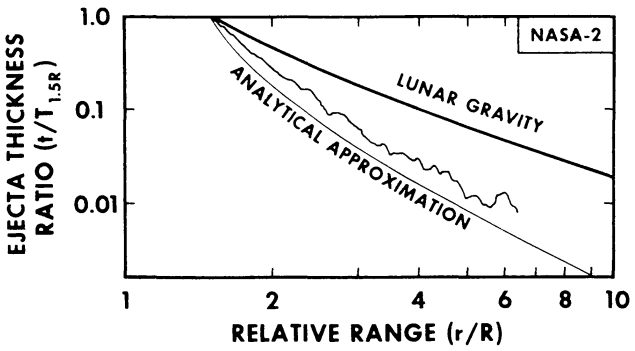

Fig. 6. The distribution of relative mass/area ("thickness," t) for NASA-2 results under terrestrial and lunar gravity. Thickness is referenced to the value at 1.5R, and distance, r, is referenced to final gravity-limited radius. Values shown represent a running mean of output data. The analytical approximation refers to a simplified model of crater growth and velocity distribution used in Schultz and Gault (1979).

effects are not considered since the primary interest here is the relative amount of material *arriving* at different distances from the crater. The data shown in Fig. 6 have been smoothed by a running mean to remove the effects of zone sizes in the calculations.

The calculations indicate that ejecta "thickness" does not follow a simple power-law decay of $(r/R)^{-3}$ as described by McGetchin *et al.* (1973). Near the crater, thickness decreases with scaled range as $(r/R)^{-4}$, whereas beyond 3R from the rim, thickness appears to decrease as $(r/R)^{-2.5}$ under conditions of 1 g. These results are consistent with other finite difference calculations (Ahrens and O'Keefe, 1978; Bryan *et al.*, 1978) and analytical descriptions of crater growth/ejection (Schultz and Gault, 1979). Schultz and Gault (1979) attribute the rapid fall-off of near-rim ejecta thicknesses to the effects of ejection position within the crater cavity. Their idealized analytical description forms a reasonable match to the finite-difference calculations. The near-rim ejecta thickness decay is consistent with the descriptions by McGetchin *et al.* (1973). The far-rim distribution differs significantly and indicates that the amount of ejecta arriving at 10R may be grossly underestimated relative to near-rim ejecta. Figure 6 also includes the idealized lunar ejecta distribution for NASA-2 ejection velocities subject to lunar gravity. The lunar crater radius was increased a factor of 1.3 according to sixth-root gravity scaling (Schmidt, 1977). As expected, the ejecta on the moon are more dispersed. Near-rim ejecta thicknesses thin as $(r/R)^{-3}$, but at large relative distances from the crater, thicknesses seem to approach an asymptotic power-law decay of $(r/R)^{-2}$. Such a relation is expected where ejection velocity decreases as $(x/R)^{-3}$ and the cumulative ejecta mass increases as $(x/R)^3$ (Schultz and Gault, 1979). At very large distances (>30R), thickness decays more rapidly than $(r/R)^{-2}$ as the finite amount of total ejected mass is reached. These calculations and theoretical predictions are supported by recent experimental analyses (Stöffler *et al.*, 1980). Moreover, re-examination of data by Ulrich *et al.* (1975) reveals that a power-law thickness decay at large ranges from South Ray Crater near Apollo 16 is more consistent with $(r/R)^{-2}$ than the previously adopted value of $(r/R)^{-3}$.

Comparisons of NASA-1 and NASA-2 indicate that the ejecta distributions are very similar within four crater radii of the rim (Fig. 7). However, NASA-1 exhibits a gradual increase in relative ejecta thicknesses between 3R and 6R with fall-off beyond 9R from the crater rim. Near 6R from the crater rim, NASA-1 exhibits a relative thickness (normalized to the thickness at 1.5R) about twice that of NASA-2. This difference may relate to both the non-cubic growth of cumulative ejecta mass beyond $x/R = 0.5$ and the effect of a lower impact velocity for NASA-1.

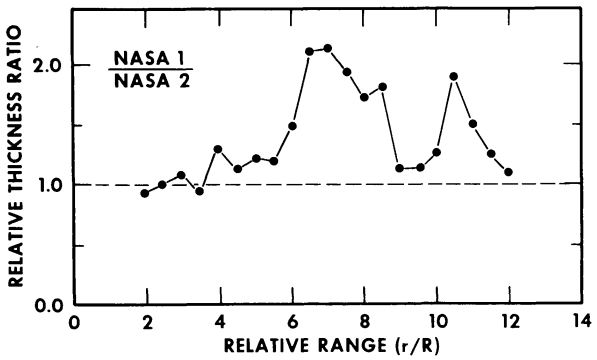

Fig. 7. The ratio of relative ejecta mass/area for NASA-1 and NASA-2 calculations as a function of range relative to the gravity-limited radius. Values shown represent a running mean of output data. An increase in relative ejecta mass/area occurs at about 6R.

POSSIBLE IMPLICATIONS FOR BASIN-SIZE EVENTS

A popular and reasonable approach for the formation of multi-ring basins *assumes* that the early stages of formation are similar to small size cratering events. Such an assumption appears to be applicable for craters over four orders of magnitude in size, i.e., between 10 cm and 1 km. Late-stage crater growth for craters much larger than 1 km is strongly influenced by gravity (Gault and Wedekind, 1977; Schmidt, 1977). Several researchers (Dence *et al.*, 1977; Gault and Wedekind, 1977; Schultz and Mendell, 1978; and Croft, 1980) have discussed the implications for gravity-controlled crater growth by impact-energy controlled shock effects. This separation between external (gravity) and internal (energy transfer) control of cratering phenomena has formed the foundation for several models of multi-ring basin formation (Dence *et al.*, 1977; Croft, 1979) where transient cavity growth is distinguished from excavation of material from the cavity. The basis for such an approach is the view that the absolute ballistic range of material is controlled by gravity, whereas the limit of the cratering flow field is controlled by material properties responding to impact energy and velocity. Therefore, extrapolation of the small cratering events to basin-size events assumes that the flow field remains essentially unchanged and that maximum transient cavity radius is limited by gravity. Such a view reconciles gravity-scaling relations for strengthless materials where diameter, D, and energy, E, are related as $D \propto E^{1/4}$ with strength-scaling relations for strength-controlled growth where $D \propto E^{1/3}$. These two scaling relations have been used to define a gravity-controlled radius, R_g, and strength-controlled radius, R_s, by various workers (Dence *et al.*, 1977; Schultz and Mendell, 1978; Croft, 1979).

The calculations described here provide a physical basis for extrapolation to basin-size events with the perspective that the multi-ring pattern represents the response of the strength-controlled disrupted crust to the gravity-controlled transient cavity limit. Specifically, results for cavity growth provide *clues* for relative transient geometry, maximum penetration, and cavity dynamics. Descriptions of the ejecta provide *clues* for trends in peak shock levels and distribution of materials around basins.

Both NASA-1 and NASA-2 indicate that crater shape and volume do not grow proportionally. The aspect ratio (diameter/depth) changes in three stages. The first stage ($x/R < 0.2$) is characterized by a rapid increase from $D/d \sim 0.6$ to near 1.0 and represents cavity growth dominated by projectile penetration. The second stage ($0.2 < x/R < 0.4$) exhibits a more gradual change in the diameter/depth values as the transient cavity diameter and depth grow somewhat proportionally. Beyond $x/R = 0.5$, the aspect ratio increases nearly linearly, a dependence reflecting constant cavity depth but enlarging crater diameter. The gravity-controlled excavation cavity with radius R_g and the strength-

controlled disruption limit with radius R_s is nearly the same for craters in the size range of NASA-1 and NASA-2. The gravity-controlled cavity of much larger craters becomes a progressively smaller fraction of the strength-controlled cavity. If the gravity-controlled excavation cavity of a basin-size event is viewed as a fraction of the transient cavity limit for NASA-1 or NASA-2 without a change in form, then we must suspect that the aspect ratio for a transient basin cavity is larger than the ratio usually extrapolated. Croft (1980) suggests that the ratio of the gravity radius to strength radius ranges from 1/6 to 1/3 for basin-size structures. Consequently, from Fig. 3, the diameter-to-depth ratio for the transient basin cavity may be less than 1.5. Such a small value would imply that the crust must adjust both vertically and laterally to a deep cylinder-like void rather than to a shallow, bowl-like cavity. If the cratering flow field is modified by the effects of gravity (e.g., see Schmidt and Holsapple, 1980) or other mechanical properties unique to high-energy impacts, then the diameter-to-depth ratio may be somewhat larger than the values inferred from simple extrapolation.

As shown in Fig. 3, the aspect ratio for the lower velocity NASA-1 calculation is significantly less than the ratio for higher velocity NASA-2 calculation. This primarily reflects the effect of maximum projectile penetration. Orphal *et al.* (1980) suggest that the calculations are consistent with the following dependence between penetration depth (p) and velocity (v) for the same physical properties of target and projectile with diameter (d):

$$p \propto d \cdot v^{2/5}.$$

If this relation is combined with strength scaling where $D \propto E^{1/3}$ and partial gravity scaling where $D \propto E^{1/3.4}$ (D = cavity diameter), then the following dependence between aspect ratios (A) are derived, respectively:

$$A \propto v^{0.27} \text{ (strength scaling)}$$

$$A' \propto v^{0.27} D^{-0.13}$$

$$A' \propto v^{0.19} d^{-0.12} = v^{0.27} D^{-0.13} \text{ (gravity scaling).}$$

At face value, these relations predict that the aspect ratio (diameter/depth) is only velocity dependent with respect to the outer strength diameter but is both velocity and diameter dependent with respect to the gravity-limited diameter. Figure 8 illustrates these

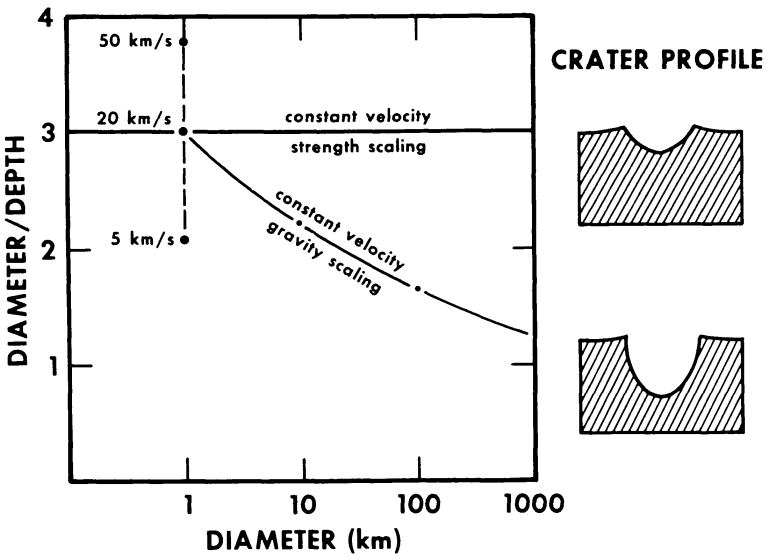

Fig. 8. Estimates of diameter:depth ratios extrapolated to basin sizes.

trends extrapolated to basin sizes. If basin-forming projectiles have relatively low velocities (<20 km/s) as suggested by (Wetherill, 1977), then the gravity-limited transient cavity conceivably could have a depth greater than its diameter. Readjustments to fill this void may trigger deep-seated rebound largely restricted to the central portion of the cavity. Such a sequence is consistent with the endogenic modification stages of multi-ring impact basins where initial and most extensive stages of modification occur within the inner ring (Schultz and Glicken, 1979; Schultz and Schultz, 1980; Dvorak and Phillips, 1980).

Figures 1 and 2 indicate that decreasing values of R_g/R_s with size also means decreasing volume fractions capable of escaping the gravity-controlled cavity due to the major role of compression rather than excavation, in the early stages of crater growth. By the time gravity limits crater growth at basin scales, the total ejected mass is less than 40% of the total displaced mass represented by the cavity. This further suggests that excavated material will be from relatively shallow horizons, in agreement with Croft's (1980) suggestion based on implications of Z-model analysis.

Several important trends are suggested by the state and distribution of ejecta. Figure 4 indicates that a wide range of peak shock pressures should be observed in the ejecta at a given relative distance from a crater but that the typical peak-shock pressures gradually increase with distance (ejection velocity). The mixture of peak shock histories is understandable from the calculated and observed flow fields during crater formation where material from various horizons is first driven downwards, then upwards along the growing cavity, thereby crossing isobars (Gault *et al.*, 1968; Orphal, 1977; Schultz and Mendell, 1978). Figure 5 suggests that an order-of-magnitude increase in impact energy results in approximately an order-of-magnitude increase in typical and maximum peak shock pressures at a given relative or absolute ballistic range (velocity). This is also implied by the scaling of total impact melt as discussed by Orphal *et al.* (1980) for this calculation and by Lange and Ahrens (1979) for other calculations. Minimum peak shock pressures are increased by a factor less than 2. Because the two calculations represent different impact momentum (factor of 3.2), complete distinction between the effects of momentum and energy must await additional calculations. Nevertheless, Figs. 4 and 5 suggest that peak shock pressures generally increase with impact energy and ballistic range (ejection velocity).

The trends observed from NASA-1 and NASA-2 have four implications for basin-size events. First, maximum and typical shock pressures at a given *relative* range increase with impact energy irrespective of gravity control. Second, because gravity permits only the early-stage material to be ejected, greater proportions of early-time and predominantly highly shocked materials will escape the cavity as suggested by Schultz and Mendell (1978). Third, the overall increase in peak and typical shock pressures at a given relative range suggests that the proportion of melting and comminution at a given scaled range increases with crater size. These trends have potential implications for the style of ejecta emplacement (Schultz and Mendenhall, 1979). Fourth, a broad mixture of peak shock pressures should be observed in the ejecta facies at any given range. Figures 5 and 6 suggest that the minimum shock pressures found at a given range may not be drastically different, but their proportion is inferred to be less as impact energy increases.

The distribution of ejecta thicknesses (mass/area) indicated in Fig. 6 contrasts with normally quoted distributions weighted to near-rim data as discussed above. This distribution also can be scaled approximately to basin-size events if the reference radius becomes the gravity-controlled radius (R_g) and if surface curvature is ignored (see Schultz and Gault, 1979). Figure 6 suggests that the ejecta thickness (areal density) mass/area arriving at 10R from the rim (R_g) is about 1% the thickness at $1.5R_g$. This is an order of magnitude more than values (0.1%) predicted by near-rim thickness-decay relations. Moreover, ejecta thickness at the Apollo 16 site should represent about 12% of the thickness near the Apennines. This is about 3 times the amount predicted by extrapolating a power-law thickness decay described by $(r/R)^{-3}$. It should be noted that the *absolute* quantity of material will be less than that normally quoted since the crater rim refers to

the gravity-controlled rim and since early-time compression reduces the fraction of material ejected. Figure 7 further suggests that a low-velocity impact may produce a distribution different from a high-velocity impact.

In the spirit of these extrapolations, the preceding discussions are combined into the scenario depicted in Fig. 9. Early stages of formation are characterized by early-time displacement without a proportional amount of material ejected and non-proportional growth of cavity shape. At the limit of gravity-controlled cavity growth, the aspect ratio

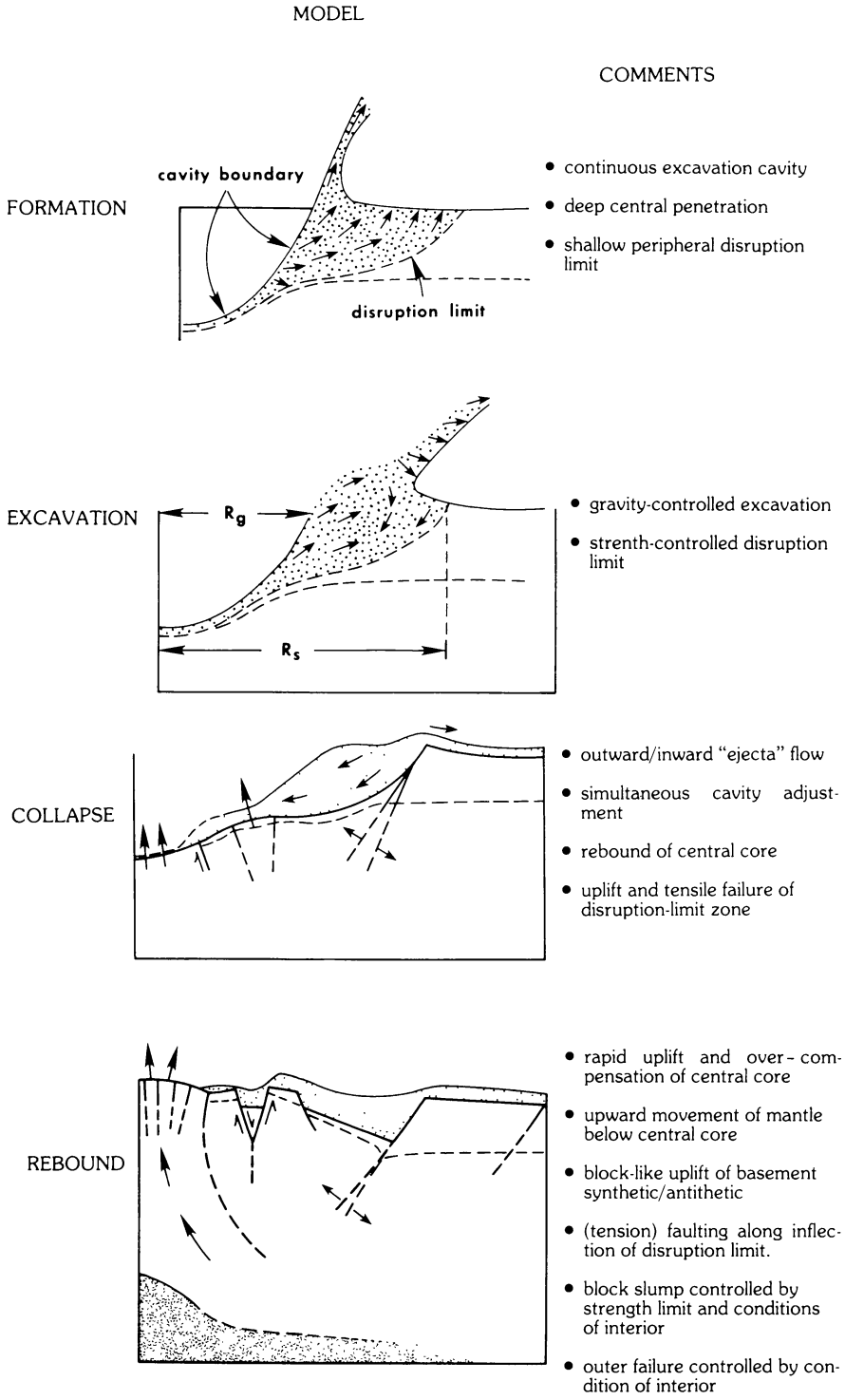

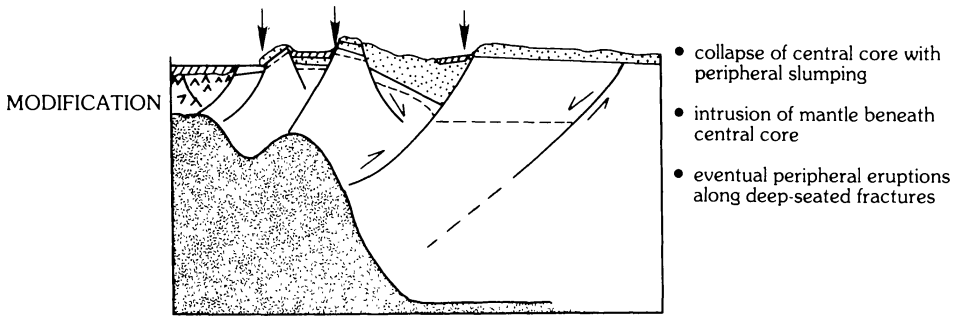

1. Central region is controlled by projectile penetration (mv/ KE) and conditions of interior
2. Second/third ring reflects uplift of disruption limit inflection with horst/graben development
3. Fourth ring delineates strength limit boundary that controls deep-seated faulting
4. Outer rings controlled by later adjustments

Fig. 9. A possible scenario for basin formation inferred from combining extrapolated calculational results, previous models, and relevant observations of basin morphology.

may be less than unity depending on the momentum/energy ratio and conditions of the interior. It seems plausible that a high-velocity (60 km/s) and relatively low density (1.0 g/cm^3) impactor would produce a significantly shallower transient cavity, thereby lessening subsequent adjustment stages. Velocity-dependent aspect ratios may help to explain the variety in multi-ring basins near the lower limit of sizes. The transient cavity represents only the limit of excavation of material, whereas the effects of shock extend to greater distances from the impact point. Material ejected beyond R_g is emplaced on a highly fractured and shock-disrupted zone contained within the strength limit R_s as discussed by Croft (1979, 1980). A slightly nested profile of the disrupted zone is illustrated in Fig. 9 and reflects observations of low-velocity impacts in sand (e.g., see Gault *et al.*, 1968) and profiles of well-preserved terrestrial impact craters such as Midland-Odessa (e.g., Short, 1965). It is important to realize that this profile is not the result of layering.

The collapse and modification stages are based on implications of the pre-collapse state and inferences from multi-ring basin morphology. As Croft (1980) suggests, the material within the strength limit is most likely dynamic, i.e., not static. Collapse of this region may be enhanced by the process of acoustic fluidization described by Melosh (1979). It is further speculated, however, that the crust cannot sustain the deep central core zone and readjusts catastrophically. Such a process could be enhanced by conditions of a thin lithosphere as proposed by Mackin (1969) and Melosh and McKinnon (1978) with elaboration by Schultz (1979) and Solomon and Head (1980). The major inner basin rings are produced by uplift of the basement and development of horsts and graben. Synthetic and antithetic faulting develops in response to central uplift and contributes to the formation of paired rings such as the Inner and Outer Rook Mountains in Orientale on the moon and the rings in Ladon on Mars. This style of ring development might account for the platform profile of many basin massifs. Moreover, the degree of inward slumping following collapse of the overcompensated central uplift and stresses related to igneous activity adds complexity to the formation and preservation of inner ring patterns. The basin center exhibits remnants of uplifted basement materials represented by hummocks that are partly exposed in Mare Orientale, are re-exposed as resistant central hummocks in eroded martian basins (Schultz and Schultz, 1980), and preserved in numerous terrestrial craters. The outer rings reflect crustal adjustments controlled by both the shock-fracture transitions and adjustments related to the state of the interior as described

by Melosh and McKinnon (1978). Arrows in Fig. 9 identify zones characterized by volcanic vents on the moon and by channel-source regions as well as ground deterioriza-tion on Mars (Schultz and Schultz, 1980). Such features are believed to reflect deep-seated fractures extending to magma reservoirs. Regions of most extensive volcanism and tectonism generally occur around the periphery of the central hummocky zone, within or at the base of massif rings, at the base of the crater ring scarp, and along a poorly defined peripheral ring beyond the ring scarp. Heavily fractured and comminuted materials not escaping the basin drape the basin interior and massifs but are superposed by subsequent volcanic units.

The essential points of the model are the following. First, the gravity-limited cavity grows non-proportionally and its form is not bowl-shaped but cylinder-shaped. Second, the aspect ratio is controlled by the velocity of the impacts. Third, the transient cavity rim may not exist as an identifiable feature following readjustment stages. Fourth, although the transient cavity may extend to great depths (200 km) in major basins, excavation is restricted to much shallower depths as Croft (1980) proposed. The present calculations suggest that even during the late stages of crater formation less than 50% of the displaced mass represented by the cavity is actually in the ejecta, thereby further decreasing relative contributions by deep horizons in the ejecta for very large basins. Fifth, basin rings represent a variety of causes related to the response of the crust to the unstable transient basin cavity and conditions of the interior. Sixth, a large fraction of material normally ejected in smaller cratering events is retained within the basin-size events and drapes uplifted basement materials.

CONCLUDING REMARKS

Cratering calculations are revealing intriguing trends. Some of these trends add weight to previous intuitions, calculations, and experimental results; others require further calculations to gain new insights. The significance of many of the trends is not fully appreciated until they are extrapolated to basin-size events. Extrapolations from NASA-1 and NASA-2 raise the following questions for the transient basin cavity:

1. Does the gravity-limited growth for basin-size events imply that the ratio of diameter to depth approaches unity, rather than shallowing to a bowl? Moreover, does the limit of disruption delineated by the cratering flow field extend to the strength limit as discussed by Croft (1980)?
2. If impact velocity is decreased for the same impact energy, does the gravity-limited transient cavity become deeper with an aspect ratio perhaps less than unity?
3. Does the adjustment of the underlying crust and surrounding shock-crushed zone within the strength limit principally respond to a deep cylinder-shaped zone in the center of the basin? Does this response result in overcompensated uplift of deep-seated material in the center, collapse of the surrounding cavity wall perhaps in a manner suggested by Croft (1979), and concentric failure of outer zones as megablocks as described by Melosh and McKinnon (1978)?
4. If compression dominates early cavity growth, how does this affect basin-size cavity dynamics?

The calculational results also raise questions for the excavation and distribution of materials:

1. As gravity controls crater growth, the proportion of ejecta volume relative to cavity volume decreases due to early-time compression. Therefore, are ejecta volumes based on transient-cavity sizes progressively overestimated at basin sizes?
2. Ejecta exhibit a wide range of peak-shock values at a given range. Calculations suggest, however, that the proportion of highly shocked and melted materials at a given relative range increases with impact energy. Although velocity may play an

important role by skewing the distribution to lower peak shock pressures for lower velocity impacts, does this trend continue for material ejected thousands of kilometers from a basin where gravity selectively permits only the higher velocity material to escape the cavity?

3. Impact melt is distributed throughout the ejecta although the largest proportions are retained within the cavity or deposited near the rim. Does this trend persist to basin sizes?
4. Although the absolute value of ejecta mass/area near the rim may be lower than previously postulated, the relative mass/area decays as $(r/R)^{-2}$ rather than $(r/R)^{-3}$, thereby increasing the relative effects of ejecta arrival at greater distances. How does this affect ejecta emplacement processes?

Based on the extrapolations, we propose a new scenario that incorporates elements of several existing basin models. We can test such extrapolations only by further testing the limitations of finite-difference codes through 1:1 comparisons with experiments (e.g., see Thomsen *et al.*, 1980; Austin *et al.*, 1980), by systematically changing the most fundamental variables of impact cratering (energy, momentum) in future calculations, and by testing the validity of extrapolations beyond human experience through experimental constraints (e.g., Schmidt and Holsapple, 1980; Greeley *et al.*, 1980).

Acknowledgments—The authors appreciate the careful and constructive reviews by Robert Schmidt and Albert Chabai. One of us (B. M.) greatly acknowledges the opportunity to perform this research as an LPI summer intern (1980). The Lunar and Planetary Institute is operated by the Universities Space Research Association under Contract No. NSR 09-051-001 with the National Aeronautics and Space Administration. This paper constitutes the Lunar and Planetary Institute Contribution No. 431.

REFERENCES

Austin J. M., Ruhl S. F., Orphal D. L., and Schultz P. H. (1980) Calculational investigation of impact cratering dynamics: Material motions during the growth period (abstract). *Lunar and Planetary Science XI*, p. 46–48. Lunar and Planetary Institute, Houston.

Ahrens T. J. and O'Keefe J. D. (1978) Energy and mass distributions of impact ejecta blankets on the moon and Mercury. *Proc. Lunar Planet. Sci. Conf. 9th*, p. 3787–3802.

Bryan J. B., Burton D. E., Cunningham M. E., and Lettis L. A. Jr. (1978). A two-dimensional computer simulation of hypervelocity impact cratering: Some preliminary results for Meteor Crater, Arizona. *Proc. Lunar Planet. Sci. Conf. 9th*, p. 3931–3964.

Croft S. K. (1979) Interplanetary basin ring spacing: Consequence of gravity vs. strength scaling (abstract)? *Lunar and Planetary Science X*, p. 248–250. Lunar and Planetary Institute, Houston.

Croft S. K. (1980) Cratering flow fields: Implications for excavation cavities, transient cavities, and depth of excavation (abstract). *Lunar and Planetary Science XI*, p. 180–182. Lunar and Planetary Institute, Houston.

Dence M. R., Grieve R. A. F., and Robertson P. B. (1977) Terrestrial impact structures: Principal characteristics and energy considerations. In *Impact and Explosion Cratering* (D. J. Roddy, R. O. Pepin, and R. B. Merrill, eds.), p. 247–275. Pergamon, N.Y.

Dvorak J. and Phillips R. J. (1980) The origin of lunar mascons; analysis of the Bouguer gravity associated with Grimaldi. In *Multi-ring Basins, Proc. Lunar Planet Sci.*, 12A (P. H. Schultz and R. B. Merrill, eds.). This volume.

Gault D. E. and Wedekind J. A. (1977) Experimental hypervelocity impact into quartz sand—II, Effects of gravitational acceleration. In *Impact and Explosion Cratering* (D. J. Roddy, R. O. Pepin, and R. B. Merrill, eds.), p. 1231–1244. Pergamon, N.Y.

Gault D. E., Quaide W. L., and Oberbeck V. R. (1968) Impact cratering mechanics and structures. In *Shock Metamorphism of Natural Materials* (B. M. French and N. M. Short, eds.), p. 87–99. Mono, Baltimore.

Greeley R., Fink J., and Gault D. E. (1980) Impact basins: Implications from experiments (abstract). In *Papers Presented to the Conference on Multi-ring Basins: Formation and Evolution*, p. 18–20. Lunar and Planetary Institute, Houston.

Lange M. A. and Ahrens T. J. (1979) Impact melting during the first 1.5 b.y. of lunar history (abstract). In *Lunar and Planetary Science X*, p. 700–702. Lunar and Planetary Institute, Houston.

Mackin J. H. (1969) Origin of lunar maria. *Bull. Geol. Soc. Amer.* **80**, 735–748.

McGetchin T. R., Settle M., and Head J. W. (1973) Radial thickness variation in impact crater ejecta: Implications for lunar basin deposits. *Earth Planet. Sci. Lett.* **20**, 226–236.

Melosh H. J. (1979) Acoustic fluidization–new geologic process. *J. Geophys. Res.* **84**, 7513–7520.
Melosh H. J. and McKinnon W. B. (1978) The mechanics of ringed basin formation. *Geophys. Res. Lett.* **5**, 985–988.
O'Keefe J. D. and Ahrens T. J. (1977) Impact-induced energy partitioning, melting, and vaporization on terrestrial planets. *Proc. Lunar Sci. Conf. 8th*, p. 3357–3374.
Orphal D. L. (1977) Calculations of explosion cratering–I. The shallow-buried nuclear detonation JOHNIE BOY. In *Impact and Explosion Cratering* (D. J. Roddy, R. O. Pepin, and R. B. Merrill, eds.), p. 897–906. Pergamon, N.Y.
Orphal D. L., Borden W. F., Larson S. A., and Schultz P. H. (1980) Impact melt generation and transport. *Proc. Lunar Planet. Sci. Conf. XI*, p. 2309–2323.
Schultz P. H. (1979) Evolution of intermediate-age impact basins on the Moon. In *Proc. Conf. Lunar Highlands Crust* (J. J. Papike and R. B. Merrill, eds.), p. 141–142. Pergamon, N.Y.
Schultz P. H. and Mendell W. (1978) Orbital infrared observations of lunar craters and possible implications for impact ejecta emplacement. *Proc. Lunar Planet. Sci. Conf. 9th*, p. 2857–2883.
Schultz P. H. and Mendenhall M. (1979) On the formation of basin secondary craters by ejecta complexes (abstract). In *Lunar and Planetary Science X*, p. 1078–1080. Lunar and Planetary Institute, Houston.
Schultz P. H. and Gault D. E. (1979) Atmospheric effects on martian ejecta emplacement. *J. Geophys. Res.* **84**, 7669–7687.
Schultz P. H. and Glicken H. (1979) Impact crater and basin control of igneous processes on Mars. *J. Geophys. Res.* **84**, 8033–8047.
Schultz P. H. and Schultz R. A. (1980) Ancient impact basins on Mars (abstract). In *Papers Presented to the Conference on Multi-ring Basins: Formation and Evolution*, p. 77–79. Lunar and Planetary Institute, Houston.
Schmidt R. M. (1977) A centrifuge cratering experiment: Development of a gravity-scaled yield parameter. In *Impact and Explosion Cratering* (D. J. Roddy, R. O. Pepin, and R. B. Merrill, eds.), p. 1261–1278. Pergamon, N.Y.
Schmidt R. M. and Holsapple K. A. (1980) Theory and experiments on centrifuge cratering. *J. Geophys. Res.* **85**, 235–252.
Short N. M. (1965) A comparison of features characteristic of nuclear explosion craters and astroblemes. *Ann. N.Y. Acad. Sci.* **123**, 573–616.
Solomon S. C. and Head J. W. (1980) Lunar mascon basins: Lava filling, tectonics, and evolution of the lithosphere. *Rev. Geophys. Space Phys.* **18**, 107–141.
Stöffler D., Gault D. E., and Reimold W. U. (1980) Cratering experiments in non-cohesive and weakly cohesive sand: Excavation mode and ejecta characteristics (abstract). In *Papers Presented to the Conference on Multi-ring Basins: Formation and Evolution*, p. 89–91. Lunar and Planetary Institute, Houston.
Thomsen J. M., Austin M. G., and Schultz P. H. (1980) The development of the ejecta plume in a laboratory-scale cratering event (abstract). In *Lunar and Planetary Science XI*, p. 1146–1148. Lunar and Planetary Institute, Houston.
Ulrich G. E., Moore H. J., Reed V. S., Wolfe E. W., and Larson K. B. (1975) Distribution of ejecta from South Ray Crater (abstract). In *Lunar Science VI*, p. 832–834. Lunar and Science Institute, Houston.
Wetherill G. W. (1977) Evolution of the earth's planetesimal swarm subsequent ot the formation of the earth and moon. *Proc. Lunar Sci. Conf. 8th*, p. 1–16.